Ultrasensitive detection and molecular imaging with magnetic nanoparticles

Jian Yang,[a] Jonathan Gunn,[b] Shivang R. Dave,[a] Miqin Zhang,[b] Y. Andrew Wang[c] and Xiaohu Gao*[a]

DOI: 10.1039/b700091j

Recent advances in nanotechnology have produced a variety of nanoparticles ranging from semiconductor quantum dots (QDs), magnetic nanoparticles (MNPs), metallic nanoparticles, to polymeric nanoparticles. Their unique electronic, magnetic, and optical properties have enabled a broad spectrum of biomedical applications such as ultrasensitive detection, medical imaging, and specific therapeutics. MNPs made from iron oxide, in particular, have attracted extensive interest and have already been used in clinical studies owing to their capability of deep-tissue imaging, non-immunogenesis, and low toxicity. In this Research Highlight article, we attempt to highlight the recent breakthroughs in MNP synthesis based on a non-hydrolytic approach, nanoparticle (NP) surface engineering, their unique structural and magnetic properties, and current applications in ultrasensitive detection and imaging with a special focus on innovative bioassays. We will also discuss our perspectives on future research directions.

Introduction

Bulk iron oxide is classified as a ferromagnetic material, which exhibits permanent magnetization in the absence of an external magnetic field. However, magnetism is highly dependent on material size. When the size of a ferromagnetic material decreases to a certain critical value (nanoparticle regime, superparamagnetic limits of common ferromagnetic materials can be found in ref. 1 and ref. 2), the thermal energy at room temperature will become sufficient to flip the electron spin directions in the absence of an external magnetic field, and will consequently randomize the particles' magnetic dipoles in a short period of time. In the presence of an external magnetic field, the MNPs respond quickly and align with an applied field, a phenomenon referred to as superparamagnetism. For biomedical applications, superparamagnetic NPs are often made of γ-Fe_2O_3 (maghemite) or Fe_3O_4 (magnetite) due to their biocompatibility. Magnetite particles can be converted to maghemite by chemical oxidization, which results in a color change from black to red-brown and a slightly reduced saturation magnetization. Owing to the dimensional similarities between MNPs and biomacromolecules, integration of the two is expected to produce major advances in molecular diagnostics, therapeutics, bioanalytical sciences, and bioengineering.[3–5] For example, recent advances have led to the development of functional superparamagnetic NPs that are covalently linked to biological molecules such as peptides, proteins, and nucleic acids.[6,7] These nanobioconjugates are well suited as contrast agents for *in vivo* magnetic resonance imaging (MRI), as carriers for drug delivery and gene therapy, as therapeutic agents for hyperthermia-based cancer treatment, and as structural scaffolds for tissue engineering.[8–14]

[a]*Department of Bioengineering, University of Washington, 1705 NE Pacific Street, Seattle, WA 98195, USA.*
E-mail: xgao@u.washington.edu;
Tel: +1 206-543-6562
[b]*Department of Material Science and Engineering, University of Washington, Seattle, WA 98195, USA*
[c]*Ocean NanoTech LLC, 700 Research Center Blvd, Fayetteville, AR 72701, USA*

MNP synthesis

Efficient synthetic routes for well-controlled MNP morphology have been one of the most sought-after goals of chemists and materials scientists. Early investigations have developed a number of methods, including vapor deposition, mechanogrinding, microemulsion, sol–gel processes, and coprecipitation of ferrous and ferric salts. Coprecipitation is currently the most common method because the resulting MNPs are highly biocompatible and cheap to produce. However, without a tedious size-selection process this technique is incapable of controlling the particle size and size distribution with nanometer precision, which is critical to many biomedical applications. Indeed, it has been demonstrated that magnetic resonance signals from MNPs with sizes spanning between 4 and 12 nm vary drastically.[15] In addition, the particle size is also one of the most important factors that affect the particle diffusion, *in vivo* biodistribution, circulation time in blood, and surface functionalities (*e.g.* curvature and number of ligands). Using highly uniform MNPs of the same size range (4–12 nm), Colvin and co-workers recently showed that magnetite particles respond to magnetic fields of low gradient in a size-dependent manner, which opens a new opportunity for the simultaneous separation of complex mixtures.[16]

Thorough characterization and understanding of MNPs' size-dependent physical and chemical properties only became available recently through the discovery of a new process for monodisperse MNP preparation, thermolysis

of iron precursors in organic solvents. Uniform MNPs can be routinely made in the size range of 5–30 nm in diameter using this procedure, although synthesis of uniform MNPs outside this range still needs improvements (Fig. 1). Alivisatos and co-workers first demonstrated this non-hydrolytic synthetic approach for MNPs by injecting metal cupferron complexes into organic surfactants at high temperature to yield maghemite NPs with a size distribution of 10–15%.[17] A burst of research activities on this subject occurred after Hyeon *et al.* optimized the synthesis of maghemite NPs using iron pentacarbonyl as the molecular precursor in the presence of oleic acid.[18] Recently, the same group showed their capability of controlling the particle size with 1 nm precision on a relatively large production scale,[19,20] which is difficult, if not impossible, to achieve with traditional aqueous-based synthetic approaches. This non-hydrolytic high-temperature procedure has also been optimized for the preparation of MNPs of different chemical compositions (such as iron, cobalt, magnetite, and an iron–platinum alloy), shapes (such as spheres, rods, and cubes), and internal structures (such as core/shell).[21–28] Although other types of high-quality NPs, such as semiconductor QDs, are prepared in a similar non-hydrolytic system, a distinct feature of MNP synthesis is the well-separated nucleation and growth steps. A thorough study by Casula and Alivisatos's group suggested that the formation of stable nuclei is considerably slower than their subsequent growth, and thus, the two phases are temporally separated, demonstrating that the reaction rate can be controlled by the nucleation rate.[29]

Although the new synthesis method based on the thermolysis of iron precursors can make MNPs of uniform sizes, which directly determine the magnetic properties, an argument in the field of life sciences was whether or not the uniform MNPs will offer new opportunities (such as more sensitive detection) over the traditional polydisperse MNPs prepared with the coprecipitation method. This is a particular concern since several types of FDA-approved MNPs made with the coprecipitation method have already produced a wealth of important clinical data. The concern was recently addressed after the successful synthesis of iron oxide particles doped with metal ions. Sun *et al.* first reported the synthesis of Mn- and Co-doped iron oxide NPs, which are monodisperse and have a cubic spinel structure.[30] These experiments suggest that besides the desired structural properties, the magnetic properties could also be readily modulated. Indeed, when transferred into aqueous buffer and applied to biological imaging, Cheon and co-workers recently found that the R_2 relaxivity of $MnFe_2O_4$ particles is 75% stronger than that of pure iron oxide NPs and is approximately 400% stronger than that of the conventional MNPs made in aqueous solution.[31] This direct comparison unambiguously demonstrated the advantage of the new thermolysis technology. Further improvement in contrast agents should have significant impact on MRI since MRI is inherently not as sensitive as other imaging modalities such as optical imaging and positron

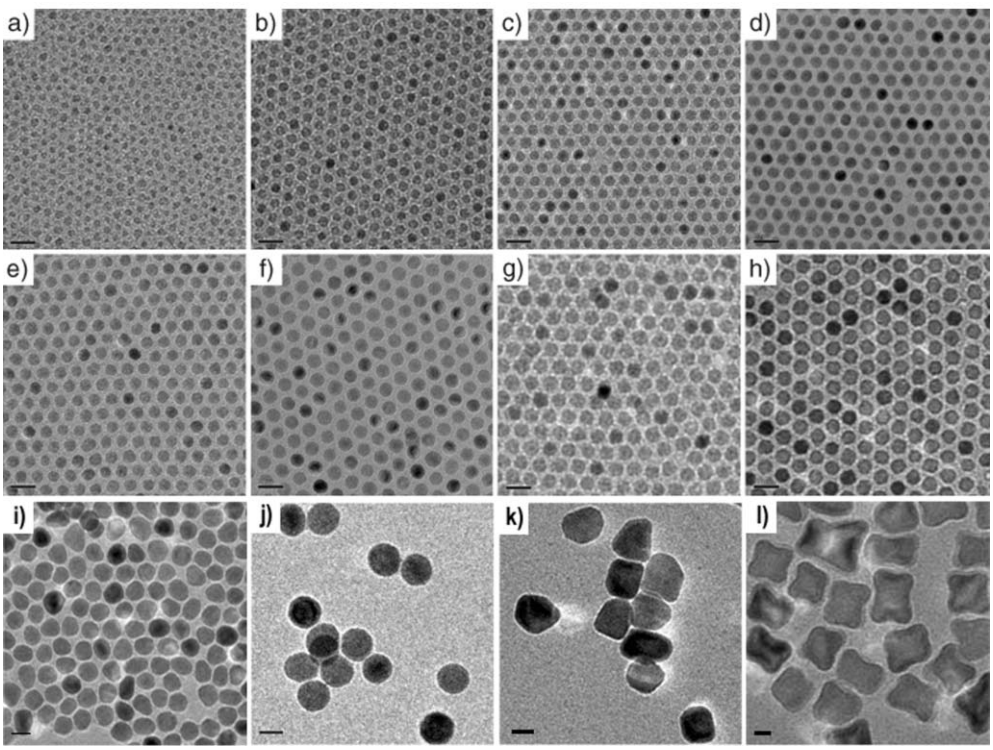

Fig. 1 TEM micrographs of (a) 6 nm-, (b) 7 nm-, (c) 8 nm-, (d) 9 nm-, (e) 10 nm-, (f) 11 nm-, (g) 12 nm-, (h) 13 nm-, (i) 20 nm-, (j) 30 nm-, (k) 40 nm- and (l) 50 nm-sized iron oxide NPs. The non-hydrolytic synthetic approach allows precise control of particle sizes. MNPs smaller than 30 nm in diameter are relatively monodisperse. Uniform MNPs of spherical shape are difficult to obtain for larger particle sizes. [Reproduced from ref. 19 (copyright 2005, Wiley InterScience).]

emission tomography (PET). An alternative approach, however, is the preparation of multimodality NPs, which has become a topic of intense research for high-resolution and high-sensitivity imaging. Recent studies show that MNPs made from Fe_2O_3 or FePt can be linked with QDs to generate dual-modality NPs.[32,33] These systems may offer detailed anatomical and molecular information when used for *in vivo* imaging of living organisms.

Surface engineering

For biological applications, the hydrophobic NPs must be made water-soluble first. Owing to the similar surface ligands of MNPs and those of QDs and gold NPs, many coating methods previously designed for QDs and gold NPs can be easily adopted for MNPs. Two general strategies have been developed to disperse MNPs in aqueous biological buffers. In the first approach, the hydrophobic monolayer of ligands on the MNP surface may be exchanged with hydrophilic ligands.[6,31] This procedure has the advantage of simplicity, but desorption of labile ligands from the MNP surface could prevent efficient conjugation with biomolecules, as ligand adsorption and desorption are likely to be reversible on the NP surface. Alternatively, hydrophobic MNPs can be rendered water-soluble with the native hydrophobic ligands retained on their surface. This is achieved through the adsorption of amphiphilic polymers that contain both a hydrophobic segment (mostly hydrocarbons) and a hydrophilic segment [such as poly(ethylene glycol) (PEG) or multiple carboxylate groups]. Several polymers have previously been reported for the surface modification of QDs, including octylamine-modified polyacrylic acid, PEG-derivatized phospholipids, block copolymers, and amphiphilic polyanhydrides.[34–37] Most of them have also been confirmed useful for modification of MNPs. The hydrophobic domains interact strongly with the alkyl chains of the ligands on the NP surface (due to the multivalency effect), whereas the hydrophilic groups face outwards and render the nanoparticles water-soluble. The biocompatibility of MNPs can be further improved by using biodegradable amphiphilic polymers originally developed for drug delivery applications.[38–40] In this design, every major component of the particle system, including the core material (*e.g.* iron oxides), particle surface ligands (*e.g.* oleic acid), and polymer coating (*e.g.* polyalkylacrylic acid and Pluronic polymers) will be biocompatible, which is of particular interest for translational research. It is also noteworthy that in comparison with the conventional dextran-coated CLIO particles (crosslinked iron oxides),[41] the new generation, water-soluble MNPs may be more compact because the amphiphilic polymer coating is thin and well-defined (Fig. 2). As a consequence, such MNPs should be more favorable in their diffusion and binding kinetics characteristics and in escaping uptake by reticuloendothelial systems when used *in vivo*. To achieve binding specificity or targeting abilities, polymer-coated MNPs are generally linked to bioaffinity ligands such as monoclonal antibodies, peptides, oligonucleotides or small-molecule inhibitors. As well, linking to poly(ethylene glycol) (PEG) or similar ligands can improve biocompatibility and reduce non-specific binding. Owing to the large surface-area to volume ratio of MNPs relative to their small-molecule counterparts (*e.g.* chelated Gd), single MNPs can be conjugated to multiple molecules for multivalent presentation of affinity tags and multifunctionality.

In vitro ultrasensitive detection

For *in vitro* applications of MNPs, an interesting phenomenon was observed by Perez, Josephson, Weissleder and coworkers that MNP aggregates are more 'potent' T_2 contrast agents than disperse MNPs of the same iron concentration. In MRI experiments, protons aligning parallel to the external magnetic field (the lowest energy state configuration) can be excited and forced away from alignment by radio-frequency pulses. The T_2 relaxation time (also known as transverse or spin–spin relaxation) is a measure of how

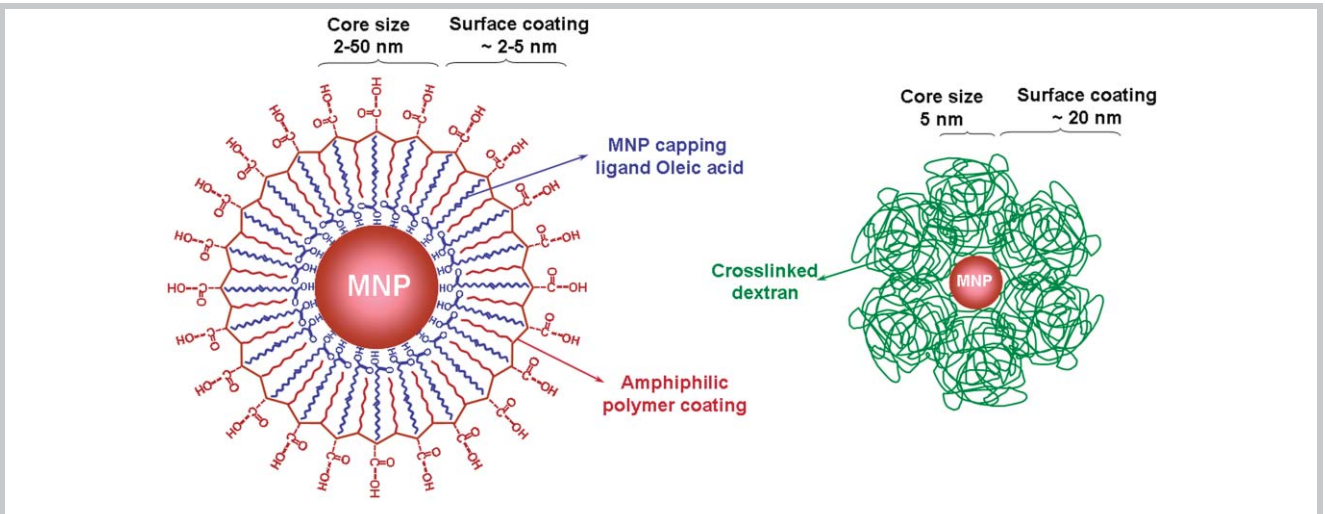

Fig. 2 Comparison of amphiphilic polymer encapsulated hydrophobic MNPs (left) and dextran-coated CLIO particles (right). The amphiphilic polymer coating is generally thin and can be made from biocompatible polymers; in contrast, the crosslinked dextran coating layer increases the particle hydrodynamic radius significantly. (Images adopted from ref. 37 and ref. 41, and re-plotted.)

long the resonating protons remain coherent or precess in-phase following a radio-frequency pulse. Although the underlying mechanism of why MNP aggregates are more efficient at dephasing the spins of surrounding water protons is not entirely clear at this time, this observation has led to the development of magnetic relaxation switching (MRS) technology for the sensitive detection of oligonucleotides, proteins, enzymes, chiral compounds, carbohydrates, and viruses with detection limits as low as 0.5 femtomoles.[42–45] In comparison with the common optical detection methods, a key essence of the MRS technology is that the magnetic relaxation changes are detectable in unpurified biological samples such as blood and turbid whole-cell lysates, which simplifies sample preparation.

A more recent trend for *in vitro* ultrasensitive detection is to integrate the high-throughput separation capability of MNPs (or MNP-doped microspheres) with an optical readout, which allows the quick separation of analytes from complex biological specimens and multiplexed quantification of the targeted molecules. Sensitive and specific detection of *Escherichia coli* O157:H7 was demonstrated by Su and Li using QDs as a fluorescence marker coupled with immunomagnetic separation. *E. coli* O157:H7 at a cell concentration of 1000 CFU ml^{-1} were detected with an assay time of less than 2 h.[46] To further enhance the detection sensitivity for low-abundance biomolecular targets, a signal amplification mechanism must be exploited, especially when the targets are proteins which cannot be amplified by the polymerase chain reaction (PCR). For example, magnetic microspheres and organic dye- or QD-doped fluorescent microspheres (serving as optical barcodes) may be combined for multiplexed detection of both DNAs and proteins. As shown in Fig. 3, a pair of molecular probes recognizing distinct domains of target molecules is linked to a fluorescent bead (multicolor) and a magnetic bead (brown). If the target DNA sequence or protein is present, it brings the two beads together, which forms a sandwich structure and can be quickly isolated using a magnet. At the same time, the fluorescent barcode reveals the identity of the target molecule. Note that the target molecules are not detected by single organic fluorophores or QDs, but by the micrometer-sized optical barcode itself, which contains thousands to millions of fluorophores. This important feature of signal amplification has the potential to bring the detection limit of both genes and proteins to the attomolar level or lower. Indeed, Groves and co-workers have showed detection of 30 aM concentrations of cytokines,[47] whereas Mirkin and co-workers demonstrated a prostate-specific antigen (PSA) detection sensitivity of less than 300 aM.[48] More importantly, the sample solution homogeneity enables substantially faster reaction kinetics than planar chips. For instance, the bridging of micrometer-sized beads by the target molecules can be accomplished in 1–2 h.[48] We envision that future research combining the multiplexing power of optical barcodes and the capability of microfluidic devices to handle samples of small volume will lead to the simultaneous detection of biomolecular targets with PCR-like sensitivity.

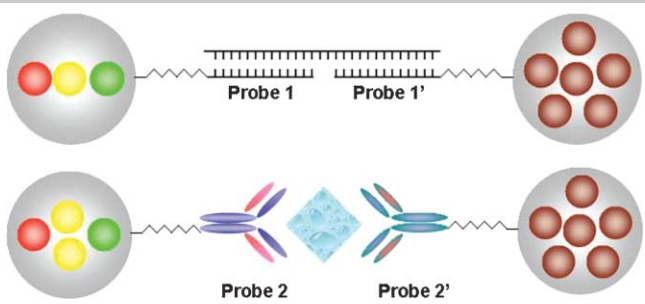

Fig. 3 Schematic illustration of DNA and protein screening applications of the magneto-optical sandwich assay. A pair of molecular probes recognizing distinct domains of target molecules is linked to an optical barcode (multicolor) and a magnetic bead (brown) for DNA (top panel) and protein (bottom panel) biomolecular target analysis. If the target is present, it brings the two beads together. After magnetic separation, the optical barcodes can be read with a spectrometer or flow cytometer at the single bead level for identification of the targets.

In vivo molecular imaging

For *in vivo* imaging, contrast agents are used in approximately 25% of MRI procedures. In the past two decades, chelated paramagnetic ions, such as Gd-DTPA, Mn(II)-EDTA, and Cr(III)-EDTA (DTPA = diethylenetriaminepentaacetic acid; EDTA = ethylenediaminetetraacetic acid), have defined the class of available *in vivo* MRI contrast agents. These chelates are resolved as bright spots against surrounding tissues as a result of their short T_1 relaxation times. In contrast to T_2 relaxation, the T_1 relaxation time (also known as longitudinal or spin–lattice relaxation) describes how quickly the 'excited' water molecules – those forced away from alignment by a 90° radio-frequency pulse – relax back to alignment. These T_1 MR contrast agents have been developed for quick removal from the vasculature, limiting long-term toxicity issues. Unfortunately, in maintaining fast excretion times, MR imaging is limited to a minimal number of scans post-injection, decreasing the overall resolution. In addition, these paramagnetic complexes have low magnetic susceptibilities, requiring the introduction of large-dose agents for sufficient contrast enhancement. To overcome the limitations associated with paramagnetic ions, MNPs have become an improved alternative to contrast agents. During MRI scans, MNPs locally disturb the induced dipolar field, shortening T_2 and, to a lesser extent, T_1 relaxation times relative to the neighboring tissue. Visually, this produces a hypointense (dark) spot in T_2-weighted scans, and hyperintense (light) spots in T_1-weighted scans.

For *in vivo* tumor imaging, MNP probes can be delivered to tumors by either a passive targeting mechanism or an active targeting mechanism. In the passive mode, macromolecules and nanometer-sized particles are accumulated preferentially at tumor sites through an enhanced permeability and retention (EPR) effect. This effect is believed to arise from two factors: (a) angiogenic tumors which produce vascular

endothelial growth factors (VEGFs) that hyperpermeabilize the tumor-associated neovasculatures and cause the leakage of circulating macromolecules and small particles; and (b) tumors lack an effective lymphatic drainage system, which leads to subsequent macromolecule or nanoparticle accumulation. Passive tumor targeting requires the MNP probes to have long plasma circulation times, which are typically achieved by shielding the MNPs with polymers such as PEG and dextran. PEG and dextran are hydrophilic polymers of low immunogenicity and can help NPs to escape from uptake by the reticuloendothelial system. For active tumor targeting, increased specificity can be attained through the immobilization of bioaffinity ligands, such as enzymes, antibodies, peptides, aptamers, and small-molecule antagonists. Ligands that have been investigated thus far include insulin, lactoferrin, ceruloplasmin, annexin V, transferrin, antibody, and folic acid. These ligands are capable of binding to receptors on the surface of the target cells. The attachment of particles to cells generally results in receptor-mediated endocytosis followed by prolonged sequestration that can be detected through MRI. Although MNPs have high promise in creating new imaging opportunities because of the myriad of available ligands and the differential receptor expression between cells types, current success in this field is mainly achieved with particles synthesized with the traditional coprecipitation method. As discussed above, this method does not produce uniform MNPs with a high magnetization level. To solve this problem, Cheon and co-workers recently showed that highly uniform $MnFe_2O_4$ NPs with significantly improved magnetic properties (*e.g.* relaxivity approximately 4× stronger than CLIO) can be made with the non-hydrolytic approach and conjugated to antibodies targeting Her-2 receptors, which makes sensitive detection of small or early-stage tumors possible. A direct comparison of the $MnFe_2O_4$ NPs and the conventional CLIO particles for *in vivo* tumor imaging is shown in Fig. 4.[31] Under the same treatment dosage, the $MnFe_2O_4$ NPs (ΔT_2 = 34%) are markedly more visible in the implanted tumors than CLIO particles ($\Delta T_2 < 5\%$).

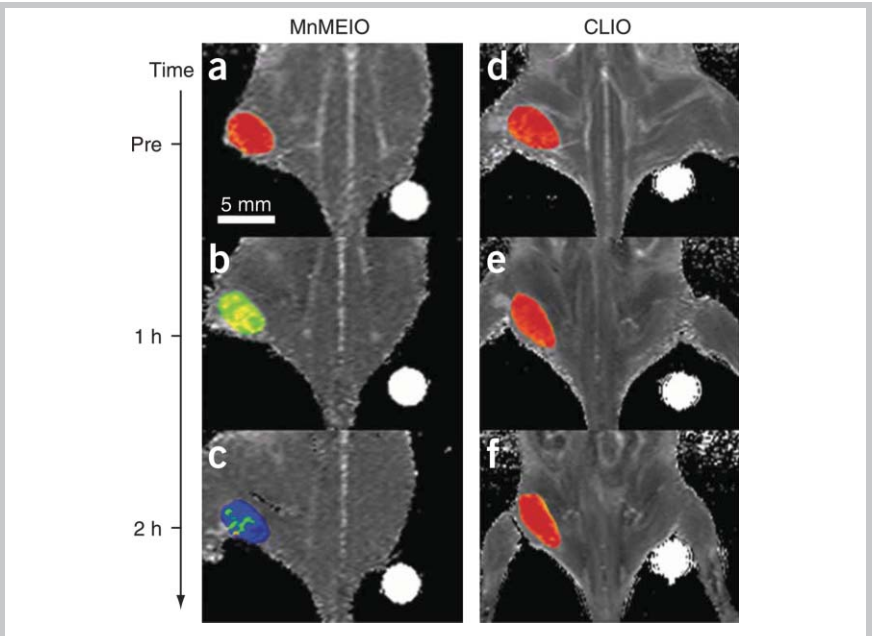

Fig. 4 *In vivo* MR detection of cancer using MNP–herceptin bioconjugates. Color maps of T_2-weighted MR images of a mouse implanted with the cancer cell line NIH3T6.7, at different time points after injection of $MnFe_2O_4$–herceptin conjugates or CLIO–herceptin conjugates [pre-injection (a,d); and 1 h (b,e) or 2 h (c,f) after injection]. In a–c, gradual color changes at the tumor site, from red (low R2) to blue (high R2), indicate progressive targeting by $MnFe_2O_4$–herceptin conjugates. In contrast, almost no change was seen in the mouse treated with the CLIO–herceptin conjugate (d–f). [MEIO = magnetism-engineered iron oxide. Reproduced from ref. 31 (copyright 2007, Nature Publishing Group).]

In vivo cell tracking

Cell tracking with magnetic NPs is desirable for *in vivo* monitoring of the administered cellular therapies. Cellular therapies use the injection of cells to improve medical conditions. Injection of endogenous dendritic or T-cells has been shown to stimulate the immune system to improve various medical conditions including cancer. Potential stem cell therapies may be used to treat a range of currently irreparable conditions such as spinal cord and myocardium injury, Parkinson's disease, multiple sclerosis, and Huntington's disease by correcting or replacing defective cell populations.[41,49] To track therapeutic cells *in vivo*, cells are first intracellularly labeled *in vitro* by endocytosis of NPs that are not cytotoxic and do not affect cellular behavior. Cells are then injected to a specific location and tracked with MRI.

The benefits of monitoring cell therapy have been demonstrated with magnetically labeled dendritic cells for melanoma therapy.[50] Dendritic cells are antigen-presenting immune cells that activate against threats such as cancer. The injection of additional dendritic cells in the lymph nodes was tracked with both magnetic and radioisotope tags. Data showed that MRI of SPIO tags (superparamagnetic iron oxide) offered markedly better resolution than scintigraphic imaging of ^{111}In radioisotopes in displaying the drainage cells from one lymph node to neighboring nodes. Additionally, MRI revealed that 50% of injections did not result in internodal cell migration because they were not administered directly into lymph node tissue but actually into nearby perinodal fat, giving a possible explanation for the limited response to the treatment in ongoing clinical trials. The reader should note that despite the many benefits of MRI, scintigraphic imaging is still the preferred method of quantified monitoring of cell migration. Most recently, Dai and co-workers prepared FeCo/single-graphitic-shell nanocrystals using the chemical vapor deposition method. The particles show outstanding relaxivity values with R1 and R2 of 70 and 644 mM^{-1} s^{-1}, respectively, which allows sensitive

tracking of mesenchymal stem cells.[51] For comparison, the R1 and R2 values of commercially available Feridex® (MNPs used in MRI for the detection of liver lesions, Advanced Magnetics) and Magnevist® (gadopentetate dimeglumine, Berlex) are only 10 and 104, and 4.6 and 4.5 mM^{-1} s^{-1}, respectively. In the growing arena of stem cell research, *in vivo* cell tracking is becoming increasingly crucial for elucidation during cellular therapy development.

MNP toxicity

Ensuring that the new MNPs are safe for use in humans is likely to be a determining factor for their impact on disease diagnosis and prognosis. As human tissue contains and metabolizes iron and iron oxides during normal functionality, including ferritin, transferrin, and hemosiderin among others, the degradation of iron oxide NPs *in vivo* is done by natural pathways leading to increased iron storage in the body. Study in rat models has demonstrated that the administration of 100 (mg Fe) kg^{-1} showed no identifiable negative effects upon the subjects, and an increase of the injected dose to 600 (mg Fe) kg^{-1} did not lead to subject death. Normal injected doses for MR contrast enhancement are significantly lower than these quantities.

While on the whole MNP variants have been shown to be relatively benign, their physiological activity does vary from system to system. For instance, Combidex® (MNPs used in MRI for differentiation of cancerous from normal lymph nodes, Advanced Magnetics) was shown to break down in intracranial tissue after three days, becoming undetectable after one week. On the other hand, Feridex® was visible under MR imaging over four weeks after administration, while demonstrating no pathological damage. At the same time, the monocrystalline iron oxide nanoparticle (MION-46) was shown to induce seizures in rats, and may not readily break down in the brain due to a lack of response from local macrophages and reactive astrocytes.[52] This demonstrates that while the major constituents of all these particles are biocompatible, size and physical coatings can induce varying physiological localization followed by diverging host responses.

Concluding remarks

Although MNPs have been used for high-throughput separation as well as clinical agents to induce hyperthemia in specifically-labeled tissues for decades, exciting new applications in bioengineering and medicine have just begun to appear in the past 3–5 years, largely triggered by recent breakthroughs in MNP synthesis and surface modification. Important progress has been made in developing functional MNPs for multiplexed separation, *in vitro* ultrasensitive detection, *in vivo* molecular imaging, and drug delivery, which will make a significant impact on the diagnosis, prognosis and treatment of complicated human diseases, such as cancer, cardiovascular diseases, and neurological disorders. Despite these recent achievements, a number of issues deserve further investigation. Although MNPs provide significantly higher contrast than gadolinium-based chelates of comparable concentration, MRI is inherently a low-sensitivity imaging modality compared with nuclear and optical imaging. As research in nanotechnology continues to generate nanomaterials with novel properties, this problem could possibly be solved by making MNPs with extremely high relaxivities, along with improvements in instrumentation (*e.g.* using a stronger magnetic field). In addition, development of compact, specifically targeted, multifunctional, and low-toxicity NP probes, and the design of innovative bioassays are in great demand, which brings both challenge and opportunity to the interdisciplinary nanotechnology research.

Acknowledgements

X. G. thanks Department of Bioengineering at the University of Washington for the new faculty startup fund and the National Science Foundation for a Faculty Early Career Development award (CAREER). S. R. D. acknowledges the National Science Foundation for generous fellowship support. This work was also partially supported by a pilot project awarded to X. G. by the Georgia Tech-Emory CCNE consortium.

References

1 K. M. Krishnan, A. B. Pakhomov, Y. Bao, P. Blomqvist, Y. Chun, M. Gonzales, K. Griffin, X. Ji and B. K. Roberts, *J. Mater. Sci.*, 2006, **41**, 793–815.
2 X. Batlle and A. Labarta, *J. Phys. D: Appl. Phys.*, 2002, **35**, R15–R42.
3 E. Katz and I. Willner, *Angew. Chem., Int. Ed.*, 2004, **43**, 6042–6108.
4 X. Gao, L. Yang, J. A. Petros, F. F. Marshall, J. W. Simons, L. Chung and S. Nie, *Curr. Opin. Biotechnol.*, 2005, **16**, 63–72.
5 D. L. Huber, *Small*, 2005, **1**, 482–501.
6 Y. M. Huh, Y. Jun, H. T. Song, S. Kim, J. Choi, J. H. Lee, S. Yoon, K. S. Kim, J. S. Shin, J. S. Suh and J. Cheon, *J. Am. Chem. Soc.*, 2005, **127**, 12387–12391.
7 R. Weissleder, K. Kelly, E. Y. Sun, T. Shtatland and L. Josephson, *Nat. Biotechnol.*, 2005, **23**, 1418–1423.
8 R. Weissleder, *Science*, 2006, **312**, 1168–1171.
9 A. Ito, M. Shinkai, H. Honda and T. Kobayashi, *J. Biosci. Bioeng.*, 2005, **100**, 1–11.
10 M. Johannsen, B. Thiesen, U. Gneveckow, K. Taymoorian, N. Waldofner, R. Scholz, S. Deger, K. Jung, S. A. Loening and A. Jordan, *Prostate*, 2006, **66**, 97–104.
11 U. Schillinger, T. Brill, C. Rudolph, S. Huth, S. Gersting, F. Krotz, J. Hirschberger, C. Bergemann and C. Plank, *J. Magn. Magn. Mater.*, 2005, **293**, 501–508.
12 A. Ito, K. Ino, M. Hayashida, T. Kobayashi, H. Matsunuma, H. Kagami, M. Ueda and H. Honda, *Tissue Eng.*, 2005, **11**, 1553–1561.
13 R. Jurgons, C. Seliger, A. Hilpert, L. Trahms, S. Odenbach and C. Alexiou, *J. Phys.: Condens. Matter*, 2006, **18**, S2893–S2902.
14 Z. Medarova, W. Pham, C. Farrar, V. Petkova and A. Moore, *Nat. Med.*, 2007, **13**, 372–377.
15 Y. W. Jun, Y. M. Huh, J. S. Choi, J. H. Lee, H. T. Song, S. Kim, S. Yoon, K. S. Kim, J. S. Shin and J. S. Suh, *J. Am. Chem. Soc.*, 2005, **127**, 5732–5733.
16 C. T. Yavuz, J. T. Mayo, W. W. Yu, A. Prakash, J. C. Falkner, S. Yean, L. Cong, H. J. Shipley, A. Kan, M. Tomson, D. Natelson and V. L. Colvin, *Science*, 2006, **314**, 964–967.
17 J. Rockenberger, E. C. Scher and A. P. Alivisatos, *J. Am. Chem. Soc.*, 1999, **121**, 11595–11596.
18 T. Hyeon, S. S. Lee, J. Park, Y. Chung and H. B. Na, *J. Am. Chem. Soc.*, 2001, **123**, 12798–12801.
19 J. Park, E. Lee, N. M. Hwang, M.S. Kang, S. C. Kim, Y. Hwang, J. G. Park, H. J. Noh, J. Y. Kim, J. H. Park and T. Hyeon, *Angew. Chem., Int. Ed.*, 2005, **44**, 2872–2877.
20 J. Park, K. An, Y. S. Hwang, J. G. Park, H. Noh, J. Kim, J. H. Park, N. Hwang and T. Hyeon, *Nat. Mater.*, 2004, **3**, 891–895.
21 N. R. Jana and X. Peng, *J. Am. Chem. Soc.*, 2003, **125**, 14280–14281.
22 F. Dumestre, B. Chaudret, C. Amiens, P. Renaud and P. Fejes, *Science*, 2004, **303**, 821–823.

23 F. Dumestre, B. Chaudret, C. Amiens, M. C. Fromen, M. J. Casanove, P. Renaud and P. Zurcher, *Angew. Chem., Int. Ed.*, 2002, **41**, 4286–4289.
24 N. O. Núñez, P. Tartaj, M. P. Morales, R. Pozas, M. Ocaña and C. J. Serna, *Chem. Mater.*, 2003, **15**, 3558–3563.
25 S. H. Sun, C. B. Murray, D. Weller, L. Folks and A. Moser, *Science*, 2000, **287**, 1989–1992.
26 C. Liu, X. Wu, T. Klemmer, N. Shukla, D. Weller, A. G. Roy, M. Tanase and D. Laughlin, *Chem. Mater.*, 2005, **17**, 620–625.
27 M. Chen, J. P. Liu and S. Sun, *J. Am. Chem. Soc.*, 2004, **126**, 8394–8395.
28 K. E. Elkins, T. S. Vedantam, J. P. Liu, H. Zeng, S. Sun, Y. Ding and Z. L. Wang, *Nano Lett.*, 2003, **3**, 1647–1649.
29 M. F. Casula, Y. Jun, D. J. Zaziski, E. M. Chan, A. Corrias and A. P. Alivisatos, *J. Am. Chem. Soc.*, 2006, **128**, 1675–1682.
30 S. Sun, H. Zeng, D. B. Robinson, S. Raoux, P. M. Rice, S. X. Wang and G. Li, *J. Am. Chem. Soc.*, 2004, **126**, 273–279.
31 J. H. Lee, Y. M. Huh, Y. W. Jun, J. W. Seo, J. T. Jang, H. T. Song, S. Kim, E. J. Cho, H. G. Yoon, J. S. Suh and J. Cheon, *Nat. Med.*, 2007, **13**, 95–99.
32 H. W. Gu, R. K. Zheng, X. X. Zhang and B. Xu, *J. Am. Chem. Soc.*, 2004, **126**, 5664–5665.
33 W. J. M. Mulder, R. Koole, R. J. Brandwijk, G. Storm, P. T. K. Chin, G. J. Strijkers, C. D. Donega, K. Nicolay and A. W. Griffioen, *Nano Lett.*, 2006, **6**, 1–6.
34 X. Y. Wu, H. J. Liu, J. Q. Liu, K. N. Haley, J. A. Treadway, J. P. Larson, N. Ge, N. F. Peale and M. P. Bruchez, *Nat. Biotechnol.*, 2003, **21**, 41–46.
35 B. Dubertret, P. Skourides, D. J. Norris, V. Noireaux, A. H. Brivanlou and A. Libchaber, *Science*, 2002, **298**, 1759–1762.
36 X. H. Gao, Y. Y. Cui, R. M. Levenson, L. W. K. Chung and S. M. Nie, *Nat. Biotechnol.*, 2004, **22**, 969–976.
37 T. Pellegrino, L. Manna, S. Kudera, T. Liedl, D. Koktysh, A. L. Rogach, S. Keller, J. Rädler, G. Natile and W. J. Parak, *Nano Lett.*, 2004, **4**, 703–707.
38 N. Murthy, J. R. Robichaud, D. A. Tirrell, P. S. Stayton and A. S. Hoffman, *J. Controlled Release*, 1999, **61**, 137–143.
39 T. K. Jain, M. A. Morales, S. K. Sahoo, D. L. Leslie-Pelecky and V. Labhasetwar, *Mol. Pharmacol.*, 2005, **2**, 194–205.
40 J. Qin, S. Laurent, Y. S. Jo, A. Roch, M. Mikhaylova, Z. M. Bhujwalla, R. N. Muller and M. Muhammed, *Adv. Mater.*, 2007, **19**, 1874–1878.
41 M. Lewin, N. Carlesso, C. H. Tung, X. W. Tang, D. Cory, D. T. Scadden and R. Weissleder, *Nat. Biotechnol.*, 2000, **18**, 410–414.
42 J. M. Perez, L. Josephson, T. O'Loughlin, D. Hogemann and R. Weissleder, *Nat. Biotechnol.*, 2002, **20**, 816–820.
43 J. M. Perez, F. J. Simeone, Y. Saeki, L. Josephson and R. Weissleder, *J. Am. Chem. Soc.*, 2003, **125**, 10192–10193.
44 A. Tsourkas, O. Hofstetter, H. Hofstetter, R. Weissleder and L. Josephson, *Angew. Chem., Int. Ed.*, 2004, **43**, 2395–2399.
45 E. Y. Sun and R. Weissleder, *Small*, 2006, **2**, 1144–1147.
46 X. L. Su and Y. Li, *Anal. Chem.*, 2004, **76**, 4806–4810.
47 J. M. Nam, A. R. Wise and J. T. Groves, *Anal. Chem.*, 2005, **77**, 6985–6988.
48 B. K. Oh, J. M. Nam, S. W. Lee and C. A. Mirkin, *Small*, 2006, **2**, 103–108.
49 J. W. M. Bulte, T. Douglas, B. Witwer, S. C. Zhang, E. Strable, B. K. Lewis, H. Zywicke, B. Miller, P. van Gelderen, B. M. Moskowitz, I. D. Duncan and J. A. Frank, *Nat. Biotechnol.*, 2001, **19**, 1141–1147.
50 I. J. M. de Vries, W. J. Lesterhuis, J. O. Barentsz, P. Verdijk, J. H. van Krieken, O. C. Boerman, W. J. G. Oyen, J. J. Bonenkamp, J. B. Boezeman, G. J. Adema, J. W. M. Bulte, T. W. J. Scheenen, C. J. A. Punt, A. Heerschap and C. G. Figdor, *Nat. Biotechnol.*, 2005, **23**, 1407–1413.
51 W. S. Seo, J. H. Lee, X. M. Sun, Y. Suzuki, D. Mann, Z. Liu, M. Terashima, P. C. Yang, M. V. McConnell, D. G. Nishimura and H. J. Dai, *Nat. Mater.*, 2006, **5**, 971–976.
52 L. L. Muldoon, M. Sandor, K. E. Pinkston and E. A. Neuwelt, *Neurosurgery*, 2005, **57**, 785–796.

